Three-dimensional niche stiffness synergizes with Wnt7a to modulate the extent of satellite cell symmetric self-renewal divisions

Louise A. Moyle[a,b,†], Richard Y. Cheng[a,b,†], Haijiao Liu[c,d], Sadegh Davoudi[a,b], Silvia A. Ferreira[e], Aliyah A. Nissar[a,b], Yu Sun[d], Eileen Gentleman[e], Craig A. Simmons[a,c,d], and Penney M. Gilbert[a,b,f,*]

[a]Institute of Biomedical Engineering, Toronto, ON M5S 3G9, Canada; [b]Donnelly Centre for Cellular and Biomolecular Research, Toronto, ON M5S 3E1, Canada; [c]Translational Biology and Engineering Program, Ted Rogers Centre for Heart Research, Toronto, ON M5G 1M1, Canada; [d]Department of Mechanical & Industrial Engineering, University of Toronto, Toronto, ON M5S 3G8, Canada; [e]Centre for Craniofacial and Regenerative Biology, King's College London, London, SE1 9RT, United Kingdom; [f]Department of Cell and Systems Biology, University of Toronto, Toronto ON, M5S 1A8, Canada

ABSTRACT **Satellite cells (SCs), the resident adult stem cells of skeletal muscle, are required for tissue repair throughout life. While many signaling pathways are known to control SC self-renewal, less is known about the mechanisms underlying the spatiotemporal control of self-renewal during skeletal muscle repair. Here, we measured biomechanical changes that accompany skeletal muscle regeneration and determined the implications on SC fate. Using atomic force microscopy, we quantified a 2.9-fold stiffening of the SC niche at time-points associated with planar-oriented symmetric self-renewal divisions. Immunohistochemical analysis confirms increased extracellular matrix deposition within the basal lamina. To test whether three-dimensional (3D) niche stiffness can alter SC behavior or fate, we embedded isolated SC-associated muscle fibers within biochemically inert agarose gels tuned to mimic native tissue stiffness. Time-lapse microscopy revealed that a stiff 3D niche significantly increased the proportion of planar-oriented divisions, without effecting SC viability, fibronectin deposition, or fate change. We then found that 3D niche stiffness synergizes with WNT7a, a biomolecule shown to control SC symmetric self-renewal divisions via the noncanonical WNT/planar cell polarity pathway, to modify stem cell pool expansion. Our results provide new insights into the role of 3D niche biomechanics in regulating SC fate choice.**

Monitoring Editor
Dennis Discher
University of Pennsylvania

Received: Feb 4, 2020
Revised: May 11, 2020
Accepted: May 26, 2020

This article was published online ahead of print in MBoC in Press (http://www.molbiolcell.org/cgi/doi/10.1091/mbc.E20-01-0078) on June 3, 2020.

†These authors contributed equally to the work.

*Address correspondence to: Penney M. Gilbert (penney.gilbert@utoronto.ca).

Abbreviations used: AFM, atomic force microscopy; $BaCl_2$, barium chloride; BCA, bicinchoninic acid; BSA, bovine serum albumin; Cryo-FESEM, Cryo-field emission scanning electron microscopy; ECM, extracellular matrix; EdU, 5-ethynyl-2′-deoxyuridine; MYOD, myogenic differentiation 1; EDL, *extensor digitorum longus*; PBS, phosphate-buffered saline; PCP, planar cell polarity; PFA, paraformaldehyde; P/S, penicillin/streptomycin; SC, satellite cell; TA, *tibialis anterior*; 3D, three dimensional; VANGL2, vang-like protein 2.

INTRODUCTION

Preserving the balance between stem cell commitment and self-renewal is critical for the long-term maintenance of tissues, none more so than skeletal muscle, which contributes 30–40% of lean body mass (Janssen *et al.*, 2000). The main stem cell population in skeletal muscle are satellite cells (SCs), a paired box transcription factor 7 (PAX7)-expressing cell located within an asymmetric niche between the muscle fiber and the basal lamina (reviewed in Relaix and Zammit, 2012). In response to injury, quiescent SCs activate, proliferate, and give rise to myoblast progenitors, which coexpress PAX7 and myogenic differentiation 1 (MYOD), before committing to differentiation, losing PAX7 expression, and fusing into multinucleated muscle fibers. Alternatively, some SCs retain $PAX7^+/MYOD^-$ status and

undergo self-renewal. Expansion of the SC stem cell pool requires symmetric division of PAX7$^+$/MYOD$^-$ cells, whereas asymmetric division of DNA and segregation of cell fate determinants gives rise to one stem cell and one myoblast. The PAX7$^+$/MYOD$^+$ myoblast then produces commitment-determined daughter cells via subsequent symmetric divisions that contribute to muscle regeneration (Shinin *et al.*, 2006; Conboy *et al.*, 2007; Kuang *et al.*, 2007; Rocheteau *et al.*, 2012; Dumont *et al.*, 2015b). While this tightly regulated process normally ensures a remarkable regenerative potential for muscle, dysregulation is associated with disease (Dumont *et al.*, 2015a; Chang *et al.*, 2016; Feige *et al.*, 2018).

There have been a growing number of studies interrogating the mechanisms that direct SC fate choice in recent years, with evidence that intrinsic and extrinsic cues play significant roles (reviewed in Dumont *et al.*, 2015b). Importantly, the asymmetric nature of the SC niche provides environmental signals that establish apicobasal cell polarity and provides orientation cues (Kuang *et al.*, 2008; Le Grand *et al.*, 2009; Bentzinger *et al.*, 2013a; Gattazzo *et al.*, 2014). Indeed, extracellular matrix (ECM) proteins of the basal lamina juxtapose with cadherins and the dystrophin glycoprotein complex of the myofiber, resulting in the differential expression of adhesion proteins on the basal and apical interfaces of the SC (reviewed in Feige *et al.*, 2018).

There is some evidence to suggest that the orientation of a SC division within the niche can determine whether a division is symmetric or asymmetric, ultimately regulating cell fate choice. Apicobasal divisions (vertical to the basal lamina) are often associated with asymmetric fate, with the self-renewing stem cell maintaining contact with the basal lamina and the myoblast progenitor retaining contact with the fiber (Kuang *et al.*, 2007; Dumont *et al.*, 2015a). One regulator of this process is the PAR complex, which orients the mitotic spindle pole; PARD3/PKCζ expression on the apical side activates p38/MAPK signaling in the myoblast (Troy *et al.*, 2012), whereas PAR1b-dystrophin complexes localize to the opposite pole (Dumont *et al.*, 2015a). Other biochemical regulators include NOTCH3 and NUMB (Conboy *et al.*, 2003; Shinin *et al.*, 2006; Kuang *et al.*, 2007). Conversely, symmetric cell divisions which result in identical daughter cells usually occur in a planar orientation. In self-renewing SC divisions, this is regulated by Wnt family member 7a (WNT7a) via the noncanonical Wnt/planar cell polarity (PCP) pathway (Le Grand *et al.*, 2009). Notably, Le Grand *et al.* (2009) offer evidence that WNT7a binding the frizzled 7 receptor (FZD7) in the myogenic factor 5 (MYF5) negative SC subpopulation polarizes vang-like protein 2 (VANGL2) expression to opposite planar poles, thereby increasing planar divisions and maintaining the stem cell pool (Le Grand *et al.*, 2009). However, this does not explain all symmetric division choices, and division orientation has not consistently been linked to fate choice in vivo (Gurevich *et al.*, 2016).

There are also a growing number of studies showing the importance of biophysical cues on SC fate; modulating matrix stiffness alters SC potency following in vitro expansion (Gilbert *et al.*, 2010), whereas continual age-related muscle stiffness impairs progenitor expansion (Lacraz *et al.*, 2015). These processes are not mutually exclusive. For example, Jagged1-specific Notch signaling synergizes with a stiff matrix to inhibit myoblast differentiation (Safaee *et al.*, 2017). In addition, several ECM proteins (including Collagen, Laminin, and Fibronectin) that tether SCs to the basal surface of their niche contribute to polarity, fate determination, and, in the case of Collagen, to mechanical stiffness (Bentzinger *et al.*, 2013b; Urciuolo *et al.*, 2013; Lukjanenko *et al.*, 2016; Tierney *et al.*, 2016; Rayagiri *et al.*, 2018; reviewed in Thomas *et al.*, 2015; Morrissey *et al.*, 2016). Furthermore, the membrane receptor integrin-β1 which forms a link between the ECM and the cytoskeleton (which is implicated in mechanotransduction) is required for the maintenance of PAX7$^+$/MYOD$^-$ self-renewing SCs (Rozo *et al.*, 2016).

An important overarching feature of these studies is that cell polarity affects division orientation, which in turn regulates symmetric versus asymmetric divisions to guide SC fate choice. However, our understanding of the mechanisms regulating symmetric cell division is limited, and the observation that the polarizing factor *Vangl2* had a stronger effect on symmetric division than *Wnt7a* suggests that *Wnt7a*-independent factors contribute to PCP (Le Grand *et al.*, 2009). One candidate could be mechanical stimuli, which has been shown to regulate VANGL2 localization and global PCP during development (Aigouy *et al.*, 2010; Ossipova *et al.*, 2015; reviewed in Gray *et al.*, 2011). Skeletal muscle is also a mechanically dynamic environment, but despite this, studies directly comparing niche forces to fate, and the mechanisms involved, are missing.

While the assessment of SCs in vivo provides a more accurate understanding of cell fate choices within the native niche, a limitation to studying the effects of altered niche stiffness arising from changes in ECM deposition or organization is that biochemical cues also alter in these pathological conditions (Conboy *et al.*, 2005; Brack *et al.*, 2007), making it difficult to unpin any biophysical consequences. Further, isolating fibers from regenerating muscle permits a retrospective analysis of cell orientation (Kuang *et al.*, 2008) which assumes that interacting cells are related. However, interpreting these findings must be carefully done, as time-lapse microscopy experiments on isolated fibers show that SCs are highly migratory and often interact with unrelated "strangers" (Siegel *et al.*, 2009, 2011). In addition, ratios of planar versus apicobasal division orientations (captured via time-lapse videos) differ between in vitro and in vivo contexts (Siegel *et al.*, 2009; Webster *et al.*, 2016), highlighting the need to identify additional layers of complexity in vitro to match in vivo outcomes.

Here, using atomic force microscopy to measure the stiffness of the SC niche, we report that the SC niche stiffens during the repair process. We then test the hypothesis that niche steric constraint, as dictated by 3D environmental stiffness, plays a crucial role in determining division orientation, which ultimately influences SC self-renewal. To mimic the transient increase in stiffness observed in the SC niche following an injury, we embedded myofiber-associated SCs in 3D agarose gels, which enabled us to model healthy and injured environments independent of cell:ECM interactions. With this artificial 3D niche system, we show that increased stiffness significantly favors SC divisions in the planar orientation without impacting SC fate. We further show that a stiff 3D niche synergizes with WNT7a to dictate the extent of self-renewal expansion divisions, thereby indicating that biophysical niche cues modulate SC fate choice.

RESULTS

The SC niche stiffens during tissue regeneration

We and others have previously shown increased muscle stiffness during regeneration (Urciuolo *et al.*, 2013; Trensz *et al.*, 2015; Safaee *et al.*, 2017), but whether this correlates to increased stiffness at the level of the SC niche is less known. Since SCs are physically located between the myofiber and the surrounding interstitium, they may be acutely sensitive to local changes in the ECM. To characterize changes of the SC niche during regeneration, we injected barium chloride ($BaCl_2$) intramuscularly into the *tibialis anterior* (TA) muscle and isolated single fibers from the adjacent *extensor digitorum longus* (EDL), which also undergoes regeneration, 7 d postinjury (Figure 1, A and B). Transgenic Pax7-zsGreen mice (Bosnakovski *et al.*, 2008) were used to visualize live SCs under the basal lamina. Atomic force microscopy (AFM) measurements revealed an apparent Young's modulus of 0.2 kPa in healthy muscle fibers, which aligns with basal

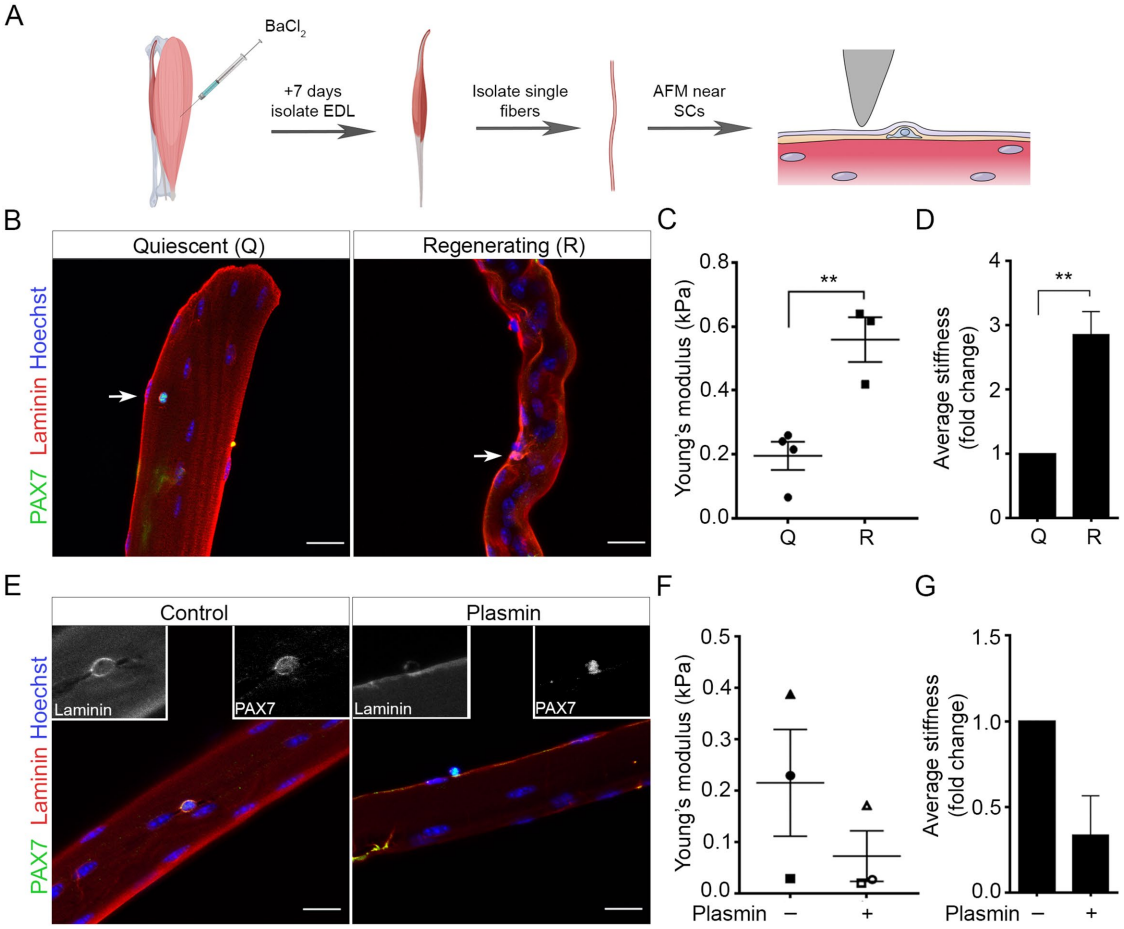

FIGURE 1: The SC niche stiffens during tissue regeneration. (A) Schematic of atomic force microscopy (AFM) method used to analyze the SC niche. *Extensor digitorum longus* (EDL) muscles were dissected from mice 7 d after intramuscular $BaCl_2$ injection into the TA muscle (Regenerating/R), or from uninjured control mice (Quiescent/Q). The EDL located beneath a $BaCl_2$-injected TA also undergoes regeneration. Single muscle fibers isolated from the EDL were subjected to AFM analysis 12 h after harvest. Created with Biorender.com (B, E) Representative confocal images of (B) Q and R fibers and (E) control and plasmin-treated fibers immediately fixed and immunostained for PAX7 (green, identifying SCs), Laminin (red, identifying basal lamina), and Hoechst (blue, nuclei). Arrows indicate SCs. Scale bars, 20 μm. (C, F) Scatter plots of AFM measurements at 5 nN indentation from (C) Q and R muscle fibers and (F) control and plasmin-treated fibers. (D, G) Bar graphs of the fold-change in stiffness of (D) Q and R muscle fibers and (G) control and plasmin-treated fibers. Scatter plots indicate fiber Young's Modulus (kPa)/ animal with lines showing the mean ± SEM; bar graphs show mean ± SEM fold-change of the average stiffness/ animal. For (C + D) Q: $N = 4$ animals (total 4 fibers) and R: $N = 3$ (total 6 fibers), $^{**}p < 0.005$, Student's unpaired *t* test. (E + F) $N = 3$ animals for control (total 3 fibers) and plasmin treatment (total 4 fibers). No significance (n.s.), Student's paired *t* test. AFM measurements were taken at multiple SC niche locations per fiber.

lamina measurements by others (Paszek *et al.*, 2005). This increased to 0.56 kPa for regenerating myofibers (Figure 1C; $p = 0.0043$), corresponding to a 2.86-fold increase in localized stiffness in the regenerating niche relative to the uninjured control (Figure 1D; $p = 0.0066$). This correlated with a localized increase in Laminin α2 expression (Figure 1B), in line with previous reports showing increased expression of other laminin isoforms (Rayagiri *et al.*, 2018) in regenerating muscle. To verify that increased stiffness results from the deposition of ECM proteins, live fibers were treated with plasmin for 1 h to degrade Laminin, Fibrin, Fibronectin and other ECM components (Liotta *et al.*, 1981; Pins *et al.*, 2000). Plasmin treatment decreased the presence of Laminin α2 (Figure 1E) and trended toward a reduction in niche stiffness fourfold compared with control fibers (Figure 1, F and G). Together, these results reveal that the local SC niche stiffens during regeneration owing, in part, to the contribution of ECM components in the basal lamina.

Tunable agarose hydrogels provide an inert three-dimensional (3D) SC niche

To understand whether mechanical stiffness directly affects SC activation and fate, we developed a methodology to embed dissociated muscle fibers in 3D artificial niches using agarose gels of varying concentrations that mimic measurements of bulk apparent moduli acquired by measuring healthy and regenerating native tissues (Figure 2A; Supplemental Figure S1) (Engler *et al.*, 2004; Gilbert *et al.*, 2010; Urciuolo *et al.*, 2013; Lacraz *et al.*, 2015; Safaee *et al.*, 2017). These stiffnesses were chosen as they more accurately recapitulate the stiffness across live muscles when all connective tissue layers are present, which is not the case in single fiber preparations. Freshly isolated fibers were equilibrated on agarose gels for 12 h at which point a top layer of agarose was added, followed by an additional 36 h of culture, during which we assessed the effect of mechanical stiffness on cell fate choice.

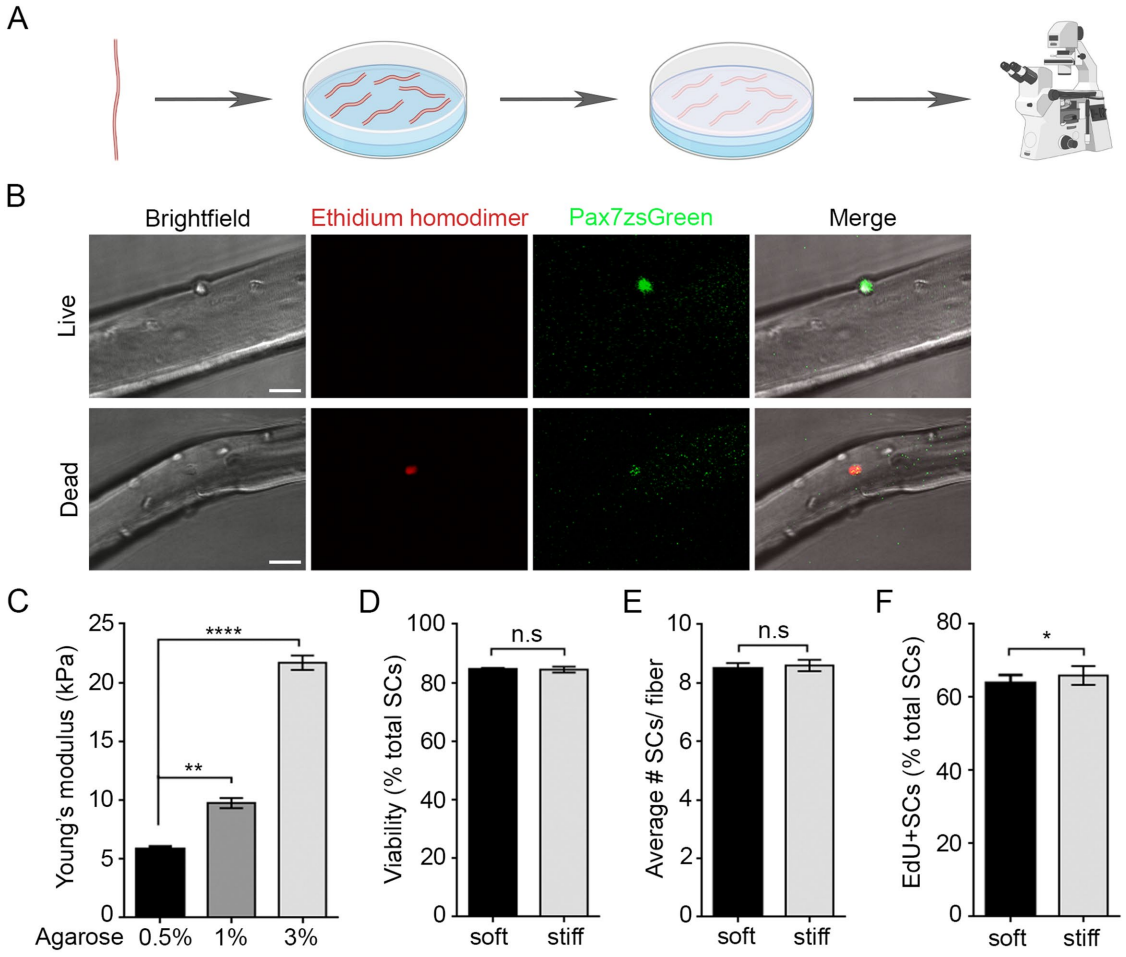

FIGURE 2: Embedding fibers within a 3D artificial niche of tunable mechanical stiffness does not alter viability or number of SCs/ fiber. (A) Schematic of experimental approach used to embed single fibers with associated SCs into 3D soft and stiff artificial niches. EDL fibers are placed atop an agarose gel layer and embedded with a top layer 12 h after isolation. SCs were tracked between 36 and 48 h after isolation. Created with Biorender.com (B) Representative confocal images of ethidium homodimer (red) staining of live (top) and dead (bottom) SCs on fibers isolated from Pax7-zsGreen transgenic mice to identify SCs embedded within soft or stiff 3D niches. Scale bar, 25 μm. (C) Bar graph of average Young's modulus (kPa) of 0.5, 1, and 3% wt/vol agarose gels quantified using compression testing. $N = 3$ gels/ condition; $^{**}p < 0.005$, $^{****}p < 0.0001$, one-way ANOVA with Tukey's multiple comparison. (D–F) Bar graphs showing mean ± SEM of soft (black) and stiff (gray) niches for (D) the percentage of viable Pax7-zsGreen$^+$ SCs that are devoid of ethidium homodimer staining 36 h after isolation (24 h after embedding). $N = 3$ animals/ condition with 10 fibers averaged per mouse (256 cells soft, 259 cells stiff), (n.s.) no significance, Student's paired t test; (E) total number of Pax7-zsGreen$^+$ SCs, $N = 3$ animals/ condition with 10 fibers averaged per mouse (256 cells soft, 259 cells stiff), (n.s.) no significance, Student's paired t test; and (F) percentage of Pax7-zsGreen$^+$ SCs that incorporated EdU between 36 and 48 h postisolation. $N = 3$ animals/ condition with 10 fibers averaged per mouse (149 cells soft, 130 cells stiff); $^*p < 0.05$, Student's paired t test.

Agarose gels were chosen as they can be mechanically tuned via weight/volume concentrations, allow for nutrient diffusion, and are relatively inert, which enables the effect of niche stiffness to be assessed separately from cell:ECM interactions (Evans and Gentleman, 2014).

We used Cryo-field emission scanning electron microscopy (Cryo-FESEM) to visualize the agarose gel network, which revealed a loose porous structure at low concentrations and a tighter mesh at high concentrations (Supplemental Figure S1D). While Cryo-FESEM cannot identify exact mesh sizes, pore sizes visualized by Cryo-FE-SEM correlate with mesh sizes measured using alternative techniques (Wen *et al.*, 2014). Compression testing revealed Young's modulus values of 5.9, 9.8, and 21.7 kPa for 0.5, 1, and 3% agarose gels, respectively (Figure 2C). We chose soft (0.5%) and stiff (3%) gels for artificial 3D niche experiments as they span the breadth of physiological bulk muscle stiffness measurements reported in healthy and regenerating tissue (Engler *et al.*, 2004; Gilbert *et al.*, 2010; Urciuolo *et al.*, 2013; Lacraz *et al.*, 2015; Safaee *et al.*, 2017). As expected, cells in stiff niches remained circular in shape and were less inclined to spread, in contrast to those cultured in soft 3D niches (Supplemental Figure S1C). Importantly, increasing stiffness did not affect SC viability; ethidium homodimer uptake revealed 84.8 and 84.5% viability in soft and stiff gels, respectively (Figure 2, B and D). Artificial niche stiffness also did not alter the total number of SCs per fiber but did result in a small increase in the ability to enter the cell cycle, from 63.9% in soft to 66.1% in a stiff niche ($p = 0.035$), as shown by 5-ethynyl-2′-deoxyuridine (EdU) incorporation (Figure 2, E and F).

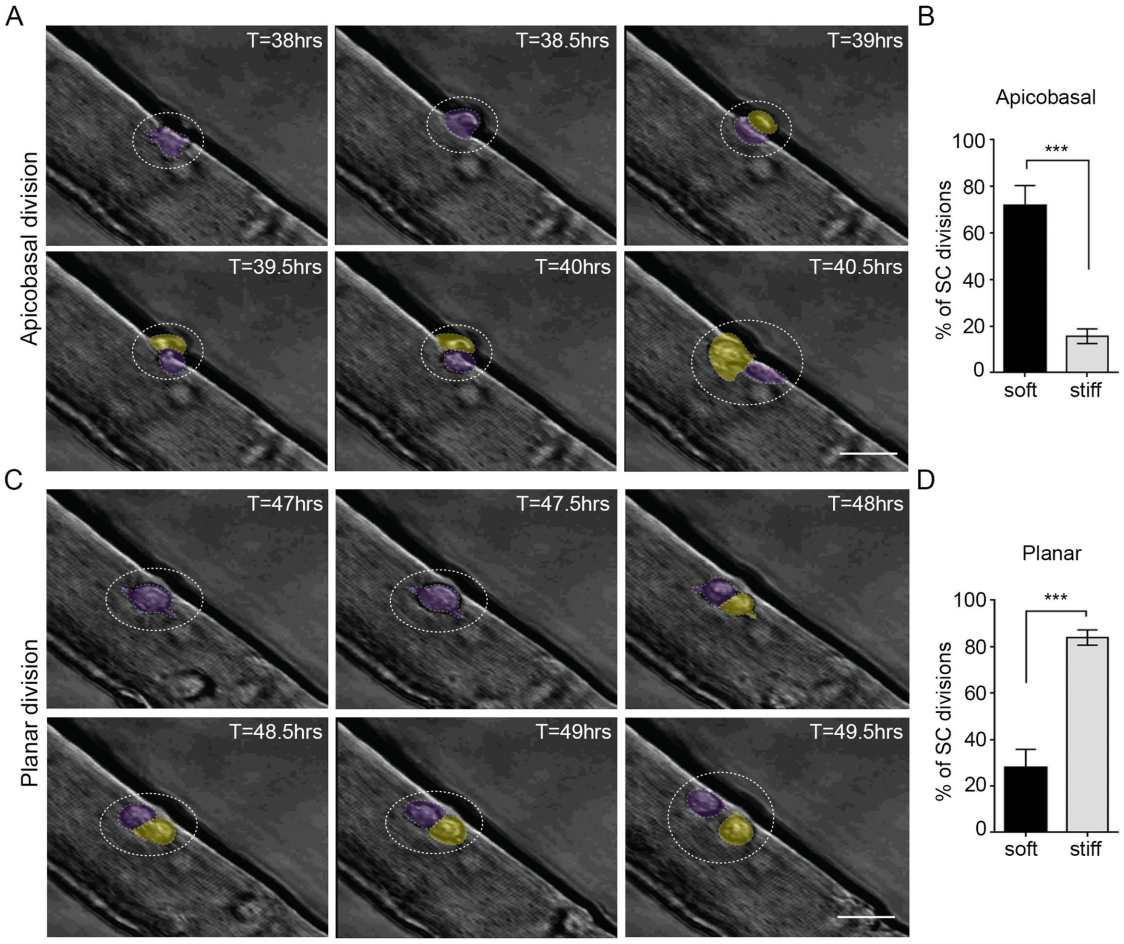

FIGURE 3: A stiff 3D niche favors planar orientation of SC division. (A, C) Still frame bright-field images from time-lapse videos showing representative (A) apicobasal and (C) planar orientation SC divisions. Scale bars, 50 µm. The "mother" cell is pseudo-colored purple and the "daughter" cell is in yellow. (B, D) Bar graphs of the average percentage of total SC divisions that occur in (B) apicobasal or (D) planar orientation when fibers are embedded within soft (black) or stiff (gray) 3D artificial niches. $N = 5$ (soft) and $N = 6$ (stiff) animals, with > 50 division instances quantified for each condition; ***$p = 0.0002$, Student's unpaired t test.

A stiff 3D niche favors planar orientation SC division

To test whether niche stiffness alone affects the orientation of the initial SC division, we conducted time-lapse microscopy on agarose-embedded fibers between 36 and 48 h after isolation (Figure 2A and Figure 3), a time frame when the first SC division occurs in most fiber-associated cells (Le Grand *et al.*, 2009; Siegel *et al.*, 2009, 2011). Images were captured every 30 min to identify the orientation of mother–daughter pairs (Figure 3, A and C). Interestingly, a stiff niche reduced the incidence of apicobasal divisions from the 71.9% observed in a soft niche down to 15.7% (Figure 3B, $p = 0.0002$). In contrast, planar division orientation, where both mother and daughter cells retain contact with the fiber, was more prevalent in stiff niches (28.1% soft and 84.3% stiff, $p = 0.0002$) (Figure 3D and Supplemental Videos S1 and S2), as determined by two independent investigators. These results suggest that SCs are more inclined to undergo apicobasal division orientations when in the context of a soft 3D environment, in contrast to a stiffened environment where they are primarily restricted to divisions in the planar orientation. In other words, niche physical properties are sufficient to influence SC division orientation.

Niche steric constraint synergizes with WNT7a to boost symmetric divisions

Orientation of SC division has been linked to division type and fate; planar orientations are associated with symmetric divisions causing SC cell pool expansion or amplification of progenitors, whereas apicobasal orientations are associated with asymmetric division and differential cell fate (reviewed in Bentzinger *et al.*, 2013a; Yin *et al.*, 2013). To determine whether niche constraint altered SC fate choice, fibers embedded in soft or stiff niches were fixed 48 h postisolation and immunostained with antibodies for PAX7 and MYOD to distinguish between stem SCs ($PAX7^+/MYOD^-$) and progenitor myoblasts ($PAX7^+/MYOD^+$) (Figure 4A, top and bottom panels, respectively). To focus our analysis on SCs that were likely to have undergone division (and thus had made a fate choice), we pulsed SCs with EdU between 36 and 48 h. As noted above, cell cycle entry was only slightly altered by niche stiffness during this time window (Figure 2F). Despite increased planar orientations of SCs in the stiff niche, we did not observe a difference in the proportion of EdU^+ SCs that expressed stem or progenitor cell signatures (Figure 4B); the percentage of $PAX7^+/MYOD^-$ stem cells was 14.2 and 10.1% in soft and stiff niches, respectively. This suggests that 3D niche stiffness alone does not affect SC fate.

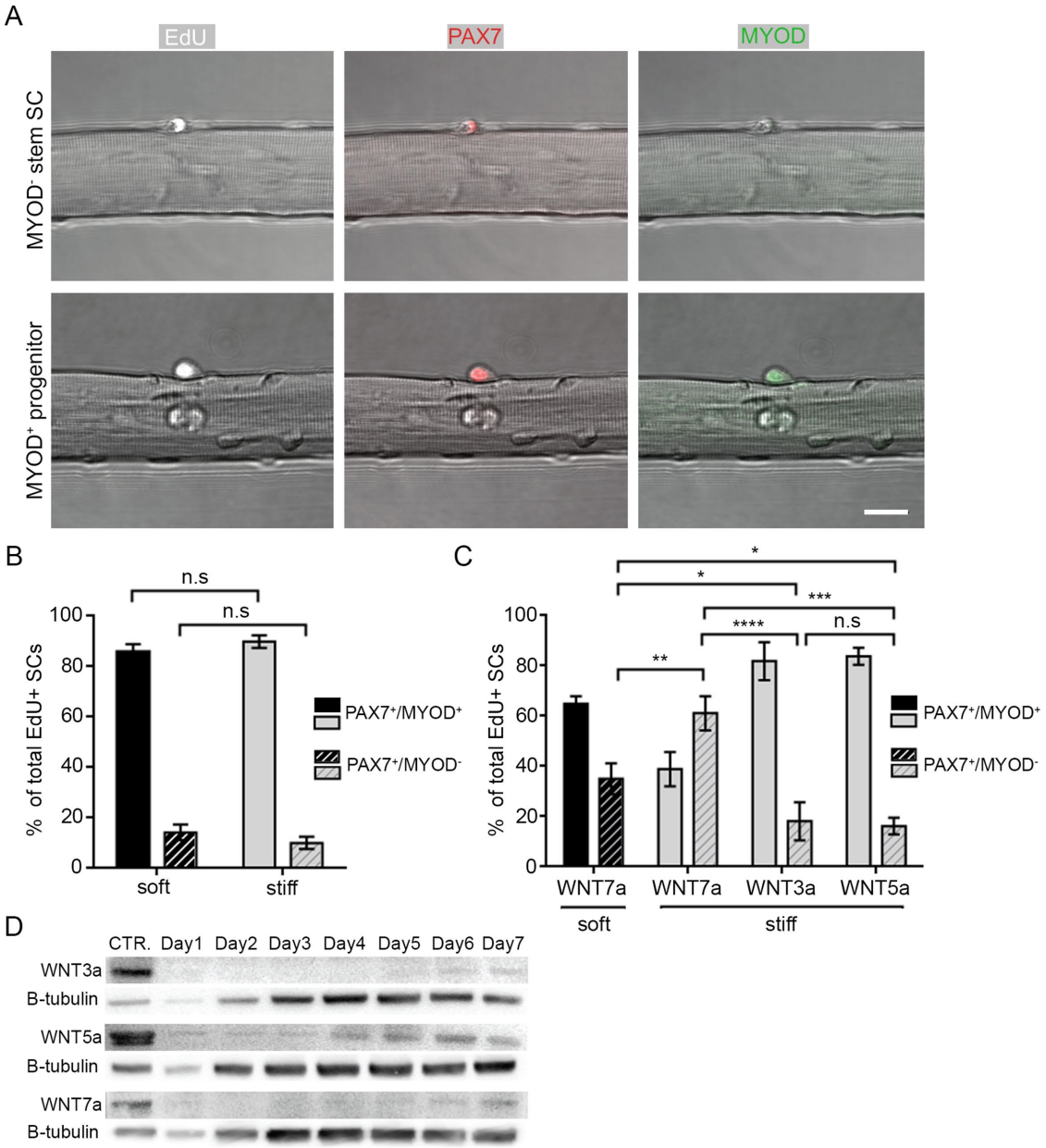

FIGURE 4: Niche steric constraint synergizes with WNT7a to boost SC symmetric stem cell pool divisions. (A) Representative confocal images of SCs on fibers pulsed with EdU 36–48 h after isolation to identify cycling cells (white) and immunostained for PAX7 (red) and MYOD (green) expression. The top panel shows a PAX7$^+$/MYOD$^-$ stem cell; the bottom panel shows a Pax7$^+$/MyoD$^+$ progenitor. Scale bar, 50 μm. (B, C) Bar graph of the percentage of PAX7$^+$/MYOD$^+$ (filled) and PAX7$^+$/MYOD$^-$ (striped) EdU$^+$ SCs in soft (black) and stiff (gray) 3D niches at 48 h after isolation in (B) control growth media or (C) with the addition of WNT3a, WNT5a, or WNT7a between 36 and 48 h post isolation. (D) Representative Western blot showing the expression of WNT3a, WNT5a, and WNT7a from TA whole lysates of uninjured (CTR.) muscles or muscles collected 1–7 d post-$BaCl_2$ injury. BCA assay was used to quantify protein and ensure equal loading. β-tubulin indicates relative changes in whole tissue cellular content at each time-point. (B, C) $N = 3$ animals/condition with ≥ 130 EdU$^+$ SCs/condition assayed; *$p < 0.05$, **$p < 0.01$, ***$p > 0.001$, ****$p > 0.0001$; (n.s.) no significance; two-way ANOVA with Tukey's multiple comparison.

Prior studies have shown that WNT7a expression is increased in regenerating muscle and specifically promotes symmetric SC division via the noncanonical Wnt/PCP pathway, boosting the stem cell pool (Le Grand *et al.*, 2009; Bentzinger *et al.*, 2013b). However, inhibiting the PCP protein VANGL2 decreased basal symmetric SC divisions, suggesting that multiple mechanisms may regulate PCP independent of WNT7a (Le Grand *et al.*, 2009). To determine if niche stiffness provides an early mechanical cue that primes SCs for WNT7a-regulated fate decisions, we added recombinant WNT7a to the culture media of myofiber-associated SCs in soft or stiff gels between 36 and 48 h (Figure 4C). Due to the relatively large mesh sizes of soft and stiff gels, we did not envisage diffusion to be impeded (Supplemental Figure S1D) (Narayanan *et al.*, 2006). As expected, the addition of WNT7a increased the proportion of PAX7$^+$/MYOD$^-$ stem cells in soft niches compared with SCs cultured without WNT ligands (Figure 4, B and C). However, SCs cultured in a stiff

niche with the addition of WNT7a further increased the percentage of stem cells, from 35.1% (soft) to 61.1% (stiff). The increased relative percentage of PAX7$^+$/MYOD$^-$ cells suggests that more symmetric self-renewing divisions (where a stem PAX7$^+$/MYOD$^-$ cell produces identical PAX7$^+$/MYOD$^-$ daughters) occurred, as opposed to symmetric divisions which resulted in two progenitor daughters (PAX7$^+$/MYOD$^+$). This is in line with previous reports (Le Grand *et al* 2009). Importantly, treatment with WNT3a and WNT5a ligands, that induce canonical Wnt/β-catenin signaling in SCs (Otto *et al.*, 2008; Le Grand *et al.*, 2009), did not alter the proportions of stem and progenitor cells in stiff niches.

Finally, we tested whether a stiff niche amplified WNT7a-induced PCP signaling through increased Fibronectin deposition, as it has been shown that Syndecan4: FZD7 binding to Fibronectin regulates WNT7a/PCP signaling in SCs (Bentzinger *et al.*, 2013b). Consistent with this report, we observed evidence of SC Fibronectin production, but a stiff niche did not appear to further elevate local Fibronectin levels (Supplemental Figure S2). Therefore, since we (Figure 4D) and others (Le Grand *et al.*, 2009) find that WNT7a protein is expressed at time-points associated with the emergence of nascent muscle fibers, we propose that biophysical cues within the regenerative SC niche (Figure 1) may synergize with WNT7a/PCP signaling to elicit a symmetric self-renewal division event prior to niche repopulation, a conclusion consistent with the increased number of quiescent SCs observed in muscle following a repair cycle (Shea *et al.*, 2010).

DISCUSSION

Studies have shown that both biochemical and biophysical cues can regulate muscle SC regeneration, but little is known about how these signals interact, or the molecular pathways involved in mechanotransduction. Here, we developed an in vitro artificial niche model to mimic increased stiffness in regenerating muscle and to determine whether this biophysical cue directly contributed to cell fate choice, independently of altered ECM expression and potential ligand accessibility.

Extending on previous findings showing increased bulk muscle stiffness in regenerating muscle (Urciuolo *et al.*, 2013; Safaee *et al.*, 2017), we utilized AFM to probe isolated muscle fibers and provide stiffness measurements at the resolution of the SC niche. Our AFM measurements of 0.2 kPa at the SC niche in healthy live murine muscle fibers are similar to previous observations (Lacraz *et al.*, 2015; Trensz *et al.*, 2015), although stiffer values have been observed in rat fibers with alternative processing (Ogneva *et al.*, 2010). Interestingly, we found that the regenerating SC niche was 2.9-fold stiffer than homeostatic, due at least in part to increased ECM deposition (Figure 1), further supporting the notion that the basal lamina remodels following SC activation (reviewed in Gattazzo *et al.*, 2014; Evano and Tajbakhsh, 2018).

Using an artificial niche model to recapitulate altered mechanical properties, we observed that a stiff niche vastly increased the proportion of planar SC divisions (Figure 3D), with incidences comparable to those reported during in vivo regeneration (Webster *et al.*, 2016), in contrast to observations of division orientation in unconstrained floating fiber cultures (Le Grand *et al.*, 2009) or fibers embedded in 2 mg/ml type I collagen (Siegel *et al.*, 2009, 2011), which is very soft (0.5 kPa for collagen gels; Joshi *et al.*, 2018).

To assess the potential cell fate consequences of increased planar divisions, we quantified the relative expression of PAX7 and MYOD in EdU$^+$ cells at 48 h after isolation, when most cells have divided (Zammit *et al.*, 2004; Siegel *et al.*, 2011). Surprisingly, division orientation alone did not affect the proportion of stem (PAX7$^+$/MYOD$^-$) and progenitor (PAX7$^+$/MYOD$^+$) cell fates, suggesting that division orientation per se does not directly determine cell fate, with regard to PAX7/MYOD expression. While we acknowledge that this is in contrast to some reports (reviewed in Feige *et al.*, 2018), there is evidence that asymmetric SC divisions are not orientation specific to the myofiber in vivo during zebrafish muscle development (Gurevich *et al.*, 2016).

Nevertheless, there is growing evidence that mechanical and biochemical cues at the SC niche act in tandem to guide cell fate (Urciuolo *et al.*, 2013; Rozo *et al.*, 2016; Safaee *et al.*, 2017; Baghdadi *et al.*, 2018; Eliazer *et al.*, 2019) (reviewed in Dumont *et al.*, 2015b; Evano and Tajbakhsh, 2018). As the Wnt/PCP pathway has been implicated in promoting planar-oriented symmetric self-renewal divisions (Le Grand *et al.*, 2009), we reasoned that increased niche stiffness might prime SCs for WNT7a-regulated fate decisions. Indeed, we demonstrate that the combination of a stiff niche and WNT7a augmented an increase to the proportion of symmetric self-renewing divisions (Figures 3 and 4), suggesting that constraint of cells within the SC niche is a biologically important feature of muscle regeneration. Notably, our finding that ECM protein deposition increases mechanical stiffness to prime SCs for symmetric cell divisions aligns with a recent study showing that deposition of laminin-111 at the basal lamina specifically induced planar-oriented symmetric self-renewal divisions (Rayagiri *et al.*, 2018). Collectively, this demonstrates that remodeling of the niche provides both mechanical and biochemical cues that contribute to maintenance of the SC pool.

Following large muscle injuries, increased stiffness at the level of the niche and consequential planar-oriented divisions are expected to occur during days 4–7 given that interstitial and basal lamina ECM proteins continue to be upregulated in the niche (Figure 1 and Safaee *et al.*, 2017), and newly differentiated muscle fibers secrete WNT7a (Figure 4D and Le Grand *et al.*, 2009). Dysregulation of these cues may alter the balance between self-renewal and progenitor expansion fate. Indeed, loss of WNT7A from myofibers leads to a reduction of the stem cell pool (Le Grand *et al.*, 2009), and one might speculate that this provides further evidence to support the notion that the continually stiff SC environment of aged or chronically injured muscle directly contributes to impaired regeneration (Lacraz *et al.*, 2015) (reviewed in Dumont *et al.*, 2015b; Dinulovic *et al.*, 2017; Li *et al.*, 2018).

It is possible that SC behavior may alter in our system compared with the native context as a consequence of collagenase digestion of the basal lamina during fiber isolation, or the continual stiffness of an artificial hydrogel niche compared with the mechanically dynamic native environment which alters during contraction and relaxation. However, we believe that embedding SC-associated fibers in artificial 3D niches recapitulates physiologically relevant biophysical cues, as evidenced by comparable levels of planar divisions (over 80%) in the stiff niche to in vivo intravital imaging (Webster *et al.*, 2016). Consequently, the effect of biophysical cues is a variable that should be taken into consideration when assessing SC fate in in vitro studies. Furthermore, our analysis of cell fate was retrospective, due to a lack of multigene reporter mouse strains to track cell fate in real time. At this timepoint (48 h) it is possible that a second SC division may have occurred in a small proportion of cells (Siegel *et al.* 2011), although the number of SCs per fiber did not alter between conditions (Figure 2E). Consequently, we were unable to track lineage relationships to quantitatively determine whether rates of asymmetric and symmetric progenitor cell divisions were affected by niche constraint. This would be an interesting avenue of future research.

In summary, this work highlights the importance of niche architecture in providing structural support in tandem with soluble cues to direct cell division orientation and myogenic progression in a spatiotemporal manner. This complements the data from Le Grand *et al*. (2009) and provides evidence that biophysical cues contribute an additional layer of cell fate control. The requirement for biochemical cues in addition to orientation-modifying steric cues provides further evidence that the regulation of cell fate is carefully controlled by the combination of spatiotemporal cues, rather than one dominant cue. This might explain why slight alterations in these environmental cues at the SC niche have drastic consequences on muscle regeneration.

MATERIALS AND METHODS

Animals

The Faculties of Medicine and Pharmacy Animal Care Committee of the Division of Comparative Medicine at the University of Toronto reviewed and approved all animal studies in this paper. C57Bl/6N wild-type mice were purchased from Charles River Laboratories (Canada). Pax7-zsGreen reporter mice were a kind gift from Michael Kyba (University of Minnesota) (Bosnakovski *et al*., 2008), and Tg(CAG-EGFP) transgenic mice were purchased from Jackson Laboratories (Okabe *et al*., 1997). Both lines were maintained in-house by backcrossing mice to C57Bl/6N, with a minimum of 10 generations of backcross into the C57Bl/6N before use in our studies. All mice used in these studies were female of 8–10 wk of age. For skeletal muscle injury studies, a single 30 µl injection of $BaCl_2$ (1.2% wt/vol in distilled H_2O; BioBasic) was delivered intramuscularly into the center of the TA muscle of anesthetized recipient animals using a 100 µl insulin syringe (BD, 324702).

Muscle fiber isolation and plasmin treatment

Single myofiber preparations were performed as described in Moyle and Zammit (2014). Briefly, the hind limbs of C57Bl/6N or Pax7-zsGreen mice were sprayed with 70% ethanol and the skin was removed to expose the underlying muscle. The attached fascia was then carefully removed and the distal tendons of both the EDL and TA were cut and the toe and ankle, respectively. The TA was lifted up and removed at the knee, before careful removal of the EDL by cutting the proximal tendons at the knee. Care was taken to delicately separate the EDL and prevent excessive stretching, which damages the integrity of the muscle fibers. Dissected EDLs were digested in DMEM (Thermo Fisher Scientific, 11995-065) containing 0.3 mg/ml of collagenase from Clostridium histolyticum (Sigma-Aldrich, C9891) for 1 h at 37°C and 5% CO_2, then rested for 30 min in 60-mm tissue culture dishes containing warm DMEM + 1% wt/vol penicillin/streptomycin (P/S; Thermo Fisher Scientific, 15140122) that had been prewashed with 5% bovine serum albumin (BSA; BioShop, ALB001.50) to prevent fibers from sticking to the dish. Individual fibers were separated by flushing the muscle with a heat-polished wide-bore glass pipette topped with a rubber bung, before being transferred to a secondary DMEM-containing dish using a narrow glass pipette, visualized with a stereomicroscope (Leica, S9E). Plates containing healthy fibers were rinsed with fresh DMEM to remove any debris and fibers were incubated in prewarmed fiber growth media, which consisted of Ham's F12 media (Thermo Fisher Scientific; 11-765-054) + 20% fetal bovine serum (FBS; Thermo Fisher Scientific, 10437028) + 1% P/S + 2.5 ng/ml basic fibroblast growth factor-2 (ImmunoTools, 11343625). The dish was then placed in the tissue culture incubator for 12 h. Dead or dying muscle fibers, as evidenced by shortened, contracted tubes, were excluded from subsequent experimental protocols. For long-term experiments, growth media exchanges were performed every 2 days. For plasmin treatment, freshly isolated fibers were incubated in growth media containing 1 nmol/l plasmin from human plasma (diluted from 100 nmol/l solutions in 0.05 M Tris-HCl; Sigma-Aldrich, P1867) for 1 h prior to atomic force microscopy measurements or fixation in 4% wt/vol paraformaldehyde (PFA; BioShop, PAR070.500).

AFM

To facilitate muscle fiber attachment to microscope slides, charged Superfrost Plus glass slides (Thermo Fisher Scientific, 12-5550-15) were coated with 50 µg/ml rat tail collagen I solution (Life Technologies, A10483-01) diluted in 0.01 N acetic acid (Sigma-Aldrich, A6285) overnight at 4°C. Excess collagen solution was removed, and slides were washed once with distilled water (MilliQ) and healthy muscle fibers from Pax7-zsGreen mice that were isolated 12 h prior were then gently placed on top of the slide surface and allowed to attach for 30 min in growth media at 37°C and 5% CO_2. AFM measurements were performed using a commercial AFM (Bioscope Catalyst, Bruker) mounted on an inverted optical microscope (Nikon Eclipse-Ti). Force-indentation measurements were completed using a trigger force of 5 nN at an indentation rate of 1 Hz using spherical tips made of borosilicate glass microspheres (15 µm radius). The cantilever (MLCT-D, Bruker) had a nominal spring constant of 0.03 N/m. AFM measurements were taken at ≥ two distinct sarcolemma regions in close proximity to a resident Pax7-zsGreen$^+$ SCs and away from myonuclei per fiber, with one to three muscle fibers averaged per mouse. For quiescent (Q) regenerating (R) muscle: Q = 4 fibers from $N = 4$ mice; R = 6 fibers from $N = 3$ mice. For plasmin treatment: control: 3 fibers from $N = 3$ mice; plasmin: 4 fibers from $N = 3$ mice.

No explicit correction for finite sample thickness effects was made between fibers. The Hertz model was applied to the force curves to estimate the contact point and apparent Young's modulus. We repeated indentation at the same location of the fiber five times and observed no significant change in the Young's moduli. Since the Young's modulus calculated from the Hertz model is sensitive to the spring constant of the AFM cantilever, cantilever spring constants were calibrated by measuring the power spectral density of the thermal noise fluctuation of the unloaded cantilever. Detailed methods are described elsewhere (Liu *et al*., 2013; Lau *et al*., 2015). All AFM measurements were completed in the fluid environment at room temperature.

3D soft and stiff artificial niches

Agarose polymer gels (0.5, 1, and 3% wt/vol) were prepared by microwaving agarose powder (BioShop, AGA001.500) in DMEM to dissolve and sterilize. Liquid agarose solution (200 µl) was added to each well of 12-well tissue culture plates (Corning, 353053) to produce the base layer. Once polymerized, gels were covered with growth media to equilibrate for 24 h at 37°C and 5% CO_2. Next, media were replaced, and muscle fibers were gently placed onto gels and allowed to stabilize for 12 h at 37°C and 5% CO_2. Media were then gently removed and a second layer of agarose solution, matching the wt/vol of the underlay and cooled to 37°C, was then added gently on top of the fibers using a P1000 pipette tip. On solidification of the second layer, growth media were added, and the plate was incubated at 37°C and 5% CO_2 incubator for several hours to equilibrate before a final media change.

Single fiber immunostaining

Muscle fibers were transferred to 2 ml optically clear microcentrifuge tubes (SSIbio, 1310-00) that had been prerinsed with 5% BSA

and fixed in 4% PFA for 15 min. For all steps, care was taken when changing solution to prevent detachment of SCs from associated fibers. Samples were triple washed in phosphate buffered saline (PBS; Sigma-Aldrich, D8662) for 5 min before permeabilization in 0.5% Triton-X100 (BioShop, TRX777.500)/PBS for 15 min. Fibers were blocked for 1 h in 10% goat serum (GS; Thermo Fisher Scientific, 16210-072)/PBS, then incubated in primary antibodies diluted in 1% GS/PBS overnight rocking at 4°C. The following primary antibodies were used: mouse anti-PAX7 hybridoma (1:5; DSHB and a kind gift from Libero Vitiello, University of Padova), rabbit anti-MYOD (1:200; Abcam, ab198251), rabbit anti-Fibronectin (1:200; Abcam, ab23750), and rat anti- Laminin 2α (1:200; Abcam ab11576). The next day, samples were triple washed in 0.025% Tween-20 (BioShop, TWN510.500)/PBS, then incubated in Alexa Fluor (Thermo Fisher Scientific) species-specific goat secondary antibodies conjugated to 488, 546, and 647 fluorophores; diluted 1:500 in 1% GS/PBS; and incubated covered from light for 1 h at room temperature. Fibers were then triple washed in 0.0025% Tween-20/PBS. Nuclei were stained ~30 min prior to confocal imaging by the addition of 1:1000 Draq5 (Abcam, ab108410) or 1:1000 Hoechst (Thermo Fisher Scientific, H3570).

Embedded fibers were processed as above with the following modifications: 4% PFA fixation time was increased to 30 min, and washes were increased to 15 min/repeat. Before overnight incubation in a modified blocking solution (0.5% Triton-X100/ 1% BSA/ PBS), individual mini gel "islands" containing muscle fibers were cut out of plates using a scalpel and placed in 2-ml microcentrifuge tubes. Gels were incubated in blocking solution on a rocker overnight at 4°C, then extensively washed and incubated in primary antibodies overnight on day 2. Secondary antibodies were incubated for 1.5 h and final 0.025% Tween-20/PBS washes were incubated for 1 h per repeat.

Confocal Z-stack images were acquired and imaged on an Olympus IX83 inverted microscope using an Olympus FluoView FV1000 confocal laser-scanning microscope. All exposure times were standardized between experimental conditions, and representative images of flattened z-stacks were projected as maximum intensity.

EdU and cell viability

In studies that assessed SC proliferation, 10 µM EdU was added to the media of 3D cultures during hours 36–48 after isolation (24 h after embedding within artificial niches). EdU was visualized after immunostaining with secondary antibodies using the Click-iT EdU Alexa Fluor-647 Imaging Kit (Thermo Fisher Scientific, C10337). Nuclear stains were added following this step.

Ethidium homodimer incorporation was performed using the LIVE/DEAD Cytotoxicity assay (Thermo Fisher Scientific, L3224) to assess cell viability 24 h postembedding.

Recombinant Wnt ligand treatment

Recombinant WNT3a (25 ng/ml; R&D Systems, 1324-WN/CF), WNT5a (25 ng/ml; R&D Systems, 645-WN/CF), or WNT7a (25 ng/ml; R&D Systems, 3008-WN/CF) proteins were added to growth media during hours 36–48 after isolation, prior to fixation.

Interface analysis

Primary myoblast cell lines were generated from Tg(CAG-EGFP) hindlimb muscles and the cultures were maintained as described before (Davoudi *et al*., 2018). Briefly, minced muscles were digested at 37°C in DMEM containing 628 U/ml collagenase Type IA collagenase (Sigma-Aldrich, C9891) for 1 h before the addition of 4.8 U/ml Dispase II (Thermo Fisher Scientific, 17105041) for a further 30 min. Digested slurry was then passed through a syringe to dissociate clumps, strained through a 40-µm filter, and incubated in red blood cell lysis buffer to remove erythrocytes. Washed and centrifuged cell pellets were then incubated with CD34 and Itgα7 antibodies to identify muscle stem cells, and the $CD34^+/Itg\alpha7^+/Sca1^-/CD45^-/CD31^-/CD11b^-$ (Thermo Fisher Scientific, eBioscience, AbLab) fraction was purified using flow cytometry assisted cell sorting. SC-derived primary myoblasts were seeded onto collagen-coated plates containing growth media and maintained at low density. To visualize the 3D hydrogel interface that single muscle fibers and associated SCs experience, we embedded $EGFP^+$ myoblasts within agarose gel layers labeled with different fluorophores; when bottom layer gel solutions reached 37°C, they were premixed 1:200 with BSA conjugated to Alexa Fluor 555 (Thermo Fisher Scientific, A34786) prior to seeding cells. Top layers of agarose were premixed with 1:200 BSA conjugated to Alexa Fluor 647 (Thermo Fisher Scientific, A34785) and then gently pipetted atop the GFP^+ myoblasts. Immediately after the top agarose gel solidified, confocal Z-stack slices 2 µm apart were acquired using FluoView software.

Cryo-FESEM

Agarose gels were placed in brass rivets, plunge frozen in a slush of liquid nitrogen at –200°C, and transferred to a cryo-stage (Gatan Alto 2500) within a JEOL JSM6301F FESEM/Oxford Inca Energy 350. Samples were fractured with a knife and surface ice was sublimated for 2 min at –90°C. Samples were then sputter coated with gold and palladium for 40 s at –140°C at an accelerating voltage of 10 kV and observed at –150°C at 15 kV. Samples were imaged at high and low magnification at least seven different regions of interest for each sample. Both gel compositions were treated and imaged in same session.

Time-lapse microscopy

To quantify SC division orientation relative to the resident muscle fiber, we performed bright-field time-lapse microscopy using an Olympus DP80 dual CCD color and monochrome camera in the context of an Olympus IX83 inverted microscope equipped with a stage-top environmental chamber to maintain physiological conditions (37°C and 5% CO_2) and a stage that raster scans to x, y coordinates. Several regions of interest were selected for each muscle fiber and multiarea time-lapse acquisition was performed using Olympus FluoView FV1000 software. Image acquisition began 24 h following muscle fiber embedding within 3D artificial niches (i.e., 36 h after fiber isolation) with images at each selected region of interest acquired at 30-min intervals for a period of 18–24 h. Images were obtained at 40× magnification and were arranged in sequential order using ImageJ software (NIH.gov) and exported as videos or still image files. Confocal Z-stack images were taken to aid in orienting the division relative to the myofiber. Division orientation was assessed manually by watching videos by two independent researchers to ensure reproducibility.

Western blot

TA muscles were isolated from control or $BaCl_2$ injured C57Bl/6N mice after 1–7 d. Muscles were lysed in RIPA buffer (Sigma-Aldrich, R0278) containing 1× Halt protease inhibitor (Thermo Fisher Scientific, 78430) and protein concentration was determined using the Pierce bicinchoninic acid (BCA) Protein Assay kit (Thermo Fisher Scientific, 23227). Either 25 µg (WNT5a, WNT7a) or 40 µg (WNT3a) of protein was loaded into an 8% bis-tris SDS–PAGE gel and run at 120 V for 2 h. The proteins were then transferred to a

nitrocellulose membrane (VWR, CA27376-991) using the Bio-Rad Transblot Turbo Transfer System (Bio-Rad, 1704155) and blocked with 5% skimmed milk (BioShop, SK1400) diluted in TBS-T (50 mM Tris-HCl/150 mM NaCl (pH 7.6)/0.1% Tween-20). Membranes were rocked overnight at 4°C with the following antibodies diluted in blocking solution: rabbit-anti WNT3a (1:500; Abcam, ab19925), rabbit-anti WNT5a (1:500; Abcam, ab72583), goat-anti WNT7a (1:500; Santa Cruz Biotechnology, sc26360), and rabbit-anti Tubulin (1:1000; Abcam, ab6046). After extensive washing in blocking solution, membranes were rocked for 60 min at room temperature with the appropriate 2° antibody diluted in blocking solution: donkey-anti goat horseradish peroxidase (HRP; 1:500; Promega, V8051) or goat-anti rabbit HRP (1:500; Cell Signaling, 7074). HRP signal was visualized using SuperSignal West Dura Extended Duration Substrate (Thermo Fisher Scientific, 34075) and the DNR Bio-Imaging Systems MicroChemi 4.2 (Israel). In cases where membranes were reprobed, the Restore PLUS Western Blot Stripping Buffer (Thermo Fisher Scientific, 46428) was used to strip blots.

Statistical analysis

All experimental procedures were performed with at least three biological replicates ($N = 3$ mice), with a minimum of three technical replicates (fibers)/animal for all experiments except AFM. For single-cell viability, proliferation, and immunofluorescence assays, we report in the legends the number of individual cells and fibers quantified in each case. Quantifications were imported in Microsoft Excel spreadsheet software and statistical tests were performed using GraphPad Prism6 statistical software. Statistical tests varied per experiment and are reported in the figure legends. For all tests, statistical significance was considered as $p \leq 0.05$.

ACKNOWLEDGMENTS

We acknowledge the following funding agencies for providing support for this work: Canada First Research Excellence Fund "Medicine by Design" Postdoctoral Fellowship, L.A.M.; Toronto Musculoskeletal Centre Fellowship, R.Y.C.; the Canadian Institutes of Health Research (GSD-128650 to A.A.N. and ONM-137370 to P.M.G.); a Philip Leverhulme Prize from the Leverhulme Trust, E.G.; the Natural Sciences and Engineering Research Council (RGPIN-4357 and RGPIN-7144 to P.M.G.); and the Human Frontiers Science Program (RGP0018/20 to P.M.G.).

REFERENCES

Aigouy B, Farhadifar R, Staple DB, Sagner A, Röper JC, Jülicher F, Eaton S (2010). Cell flow reorients the axis of planar polarity in the wing epithelium of Drosophila. Cell 142, 773–786.

Baghdadi MB, Castel D, Machado L, Fukada S, Birk DE, Relaix F, Tajbakhsh S, Mourikis P (2018). Reciprocal signalling by Notch–Collagen V–CALCR retains muscle stem cells in their niche. Nature 557, 714–718.

Bentzinger CF, Wang YX, Dumont NA, Rudnicki MA (2013a). Cellular dynamics in the muscle satellite cell niche. Nat Publ Gr 14, 1062–1072.

Bentzinger CF, Wang YX, Von Maltzahn J, Soleimani VD, Yin H, Rudnicki MA (2013b). Fibronectin regulates Wnt7a signaling and satellite cell expansion. Cell Stem Cell 12, 75–87.

Bosnakovski D, Xu Z, Li W, Thet S, Cleaver O, Perlingeiro RCR, Kyba M (2008). Prospective isolation of skeletal muscle stem cells with a Pax7 Reporter. Stem Cells 26, 3194–3204.

Brack AS, Conboy MJ, Roy S, Lee M, Kuo CJ, Keller C, Rando TA (2007). Increased Wnt signaling during aging alters muscle stem cell fate and increases fibrosis. Science (80-) 317, 807–810.

Chang NC, Chevalier FP, Rudnicki MA (2016). Satellite cells in muscular dystrophy - lost in polarity. Trends Mol Med 22, 479–496.

Conboy IM, Conboy MJ, Smythe GM, Rando TA (2003). Notch-mediated restoration of regenerative potential to aged muscle. Science 302, 1575–1577.

Conboy IM, Conboy MJ, Wagers AJ, Girma ER, Weismann IL, Rando TA (2005). Rejuvenation of aged progenitor cells by exposure to a young systemic environment. Nature 433, 760–764.

Conboy MJ, Karasov AO, Rando TA (2007). High incidence of non-random template strand segregation and asymmetric fate determination in dividing stem cells and their progeny. PLoS Biol 5, e102.

Davoudi S, Chin C-Y, Cooke MJ, Tam RY, Shoichet MS, Gilbert PM (2018). Muscle stem cell intramuscular delivery within hyaluronan methylcellulose improves engraftment efficiency and dispersion. Biomaterials 173, 34–46.

Dinulovic I, Furrer R, Handschin C (2017). Plasticity of the muscle stem cell microenvironment. In: Advances in Experimental Medicine and Biology, New York: Springer, 141–169.

Dumont NA, Wang YX, Rudnicki MA (2015b). Intrinsic and extrinsic mechanisms regulating satellite cell function. Development 142, 1572–1581.

Eliazer S, Muncie JM, Christensen J, Sun X, D'Urso RS, Weaver VM, Brack AS (2019). Wnt4 from the niche controls the mechano-properties and quiescent state of muscle stem cells. Cell Stem Cell 25, 654-665.e4.

Engler AJ, Griffin MA, Sen S, Bönnemann CG, Sweeney HL, Discher DE (2004). Myotubes differentiate optimally on substrates with tissue-like stiffness. J Cell Biol 166, 877–887.

Evano B, Tajbakhsh S (2018). Skeletal muscle stem cells in comfort and stress. NPJ Regen Med 3, 24.

Evans ND, Gentleman E (2014). The role of material structure and mechanical properties in cell-matrix interactions. J Mater Chem B 2, 2345–2356.

Feige P, Brun CE, Ritso M, Rudnicki MA (2018). Orienting muscle stem cells for regeneration in homeostasis, aging, and disease. Cell Stem Cell 23, 653–664.

Gattazzo F, Urciuolo A, Bonaldo P (2014). Extracellular matrix: A dynamic microenvironment for stem cell niche. Biochim Biophys Acta - Gen Subj 1840, 2506–2519.

Gilbert PM, Havenstrite KL, Magnusson KEG, Sacco A, Leonardi NA, Kraft P, Nguyen NK, Thrun S, Lutolf MP, Blau HM (2010). Substrate elasticity regulates skeletal muscle stem cell self-renewal in culture. Science 329, 1078–1081.

Gray RS, Roszko I, Solnica-Krezel L (2011). Planar cell polarity: coordinating morphogenetic cell behaviors with embryonic polarity. Dev Cell 21, 120–133.

Gurevich DB, Nguyen PD, Siegel AL, Ehrlich OV, Sonntag C, Phan JMN, Berger S, Ratnayake D, Hersey L, Berger J, *et al.* (2016). Asymmetric division of clonal muscle stem cells coordinates muscle regeneration in vivo. Science 353.

Janssen I, Heymsfield SB, Wang ZM, Ross R (2000). Skeletal muscle mass and distribution in 468 men and women aged 18-88 yr. J Appl Physiol 89, 81–88.

Joshi J, Mahajan G, Kothapalli CR (2018). Three-dimensional collagenous niche and azacytidine selectively promote time-dependent cardiomyogenesis from human bone marrow-derived MSC spheroids. Biotechnol Bioeng 115, 2013–2026.

Kuang S, Gillespie MA, Rudnicki MA (2008). Niche regulation of muscle satellite cell self-renewal and differentiation. Cell Stem Cell 2, 22–31.

Kuang S, Kuroda K, Le Grand F, Rudnicki MA (2007). Asymmetric self-renewal and commitment of satellite stem cells in muscle. Cell 129, 999–1010.

Lacraz G, Rouleau A-J, Couture V, Söllrald T, Drouin G, Veillette N, Grandbois M, Grenier G (2015). Increased stiffness in aged skeletal muscle impairs muscle progenitor cell proliferative activity. PLoS One 10, e0136217.

Lau K, Tao K, Liu H, Wen J, Sturgeon K, Sorfazlian N, Lazic S, Burrows JTA, Wong MD, Li D, *et al.* (2015). Anisotropic stress orients remodelling of mammalian limb bud ectoderm. Nat Cell Biol 17, 569–579.

Le Grand F, Jones AE, Seale V, Scime A, Rudnicki MA (2009). Wnt7a activates the planar cell polarity pathway to drive the symmetric expansion of satellite stem cells. Cell Stem Cell 4, 535–547.

Li EW, McKee-Muir OC, Gilbert PM (2018). Cellular biomechanics in skeletal muscle regeneration. In: Current Topics in Developmental Biology, New York: Elsevier, 125–176.

Liotta LA, Goldfarb RH, Brundage R, Siegal GP, Terranova V, Garbisa S (1981). Effect of plasminogen activator (urokinase), plasmin, and thrombin on glycoprotein and collagenous components of basement membrane. Cancer Res 41, 4629–4636.

Liu H, Sun Y, Simmons CA (2013). Determination of local and global elastic moduli of valve interstitial cells cultured on soft substrates. J Biomech 46, 1967–1971.

Lukjanenko L, *et al.* (2016). Loss of fibronectin from the aged stem cell niche affects the regenerative capacity of skeletal muscle in mice. Nat Med 22, 897–905.

Morrissey JB, Cheng RY, Davoudi S, Gilbert PM (2016). Biomechanical origins of muscle stem cell signal transduction. J Mol Biol 428, 1441–1454.
Moyle LA, Zammit PS (2014). Isolation, culture and immunostaining of skeletal muscle fibres to study myogenic progression in satellite cells. Methods Mol Biol 1210, 63–78.
Narayanan J, Xiong JY, Liu XY (2006). Determination of agarose gel pore size: Absorbance measurements vis a vis other techniques. J Phys Conf Ser 28, 83–86.
Ogneva IV, Lebedev DV, Shenkman BS (2010). Transversal stiffness and young's modulus of single fibers from rat soleus muscle probed by atomic force microscopy. Biophys J 98, 418–424.
Okabe M, Ikawa M, Kominami K, Nakanishi T, Nishimune Y (1997). "Green mice" as a source of ubiquitous green cells. FEBS Lett 407, 313–319.
Ossipova O, Kim K, Soko SY (2015). Planar polarization of vangl2 in the vertebrate neural plate is controlled by wnt and myosin II signaling. Biol Open 4, 722–730.
Otto A, Schmidt C, Luke G, Allen S, Valasek P, Muntoni F, Lawrence-Watt D, Patel K (2008). Canonical Wnt signalling induces satellite-cell proliferation during adult skeletal muscle regeneration. J Cell Sci 121, 2939–2950.
Paszek MJ, Zahir N, Johnson KR, Lakins JR, Rozenberg GI, Gefen A, Reinhart-King CA, Margulies SS, Dembo M, Boettiger D, *et al*. (2005). Tensional homeostasis and the malignant phenotype. Cancer Cell 8, 241–254.
Pins GD, Collins-Pavao ME, Van De Water L, Yarmush ML, Morgan JR (2000). Plasmin triggers rapid contraction and degradation of fibroblast-populated collagen lattices. J Invest Dermatol 114, 647–653.
Rayagiri SS, Ranaldi D, Raven A, Mohamad Azhar NIF, Lefebvre O, Zammit PS, Borycki A-GG (2018). Basal lamina remodeling at the skeletal muscle stem cell niche mediates stem cell self-renewal. Nat Commun 9, 1075.
Relaix F, Zammit PS (2012). Satellite cells are essential for skeletal muscle regeneration: the cell on the edge returns centre stage. Development 139, 2845–2856.
Rocheteau P, Gayraud-Morel B, Siegl-Cachedenier I, Blasco MA, Tajbakhsh S (2012). A subpopulation of adult skeletal muscle stem cells retains all template DNA strands after cell division. Cell 148, 112–125.
Rozo M, Li L, Fan C-M (2016). Targeting β1-integrin signaling enhances regeneration in aged and dystrophic muscle in mice. Nat Med 22, 889–896.
Safaee H, Bakooshli MA, Davoudi S, Cheng RY, Martowirogo AJ, Li EW, Simmons CA, Gilbert PM (2017). Tethered jagged-1 synergizes with culture substrate stiffness to modulate notch-induced myogenic progenitor differentiation. Cell Mol Bioeng 10, 501–513.
Shea KL, Xiang W, LaPorta VS, Licht JD, Keller C, Basson MA, Brack AS (2010). Sprouty1 regulates reversible quiescence of a self-renewing adult muscle stem cell pool during regeneration. Cell Stem Cell 6, 117–129.
Shinin V, Gayraud-Morel B, Gomès D, Tajbakhsh S (2006). Asymmetric division and cosegregation of template DNA strands in adult muscle satellite cells. Nat Cell Biol 8, 677–682.
Siegel AL, Atchison K, Fisher KE, Davis GE, Cornelison DDW (2009). 3D Timelapse analysis of muscle satellite cell motility. Stem Cells 27, 2527–2538.
Siegel AL, Kuhlmann PK, Cornelison D (2011). Muscle satellite cell proliferation and association: new insights from myofiber time-lapse imaging. Skelet Muscle 1, 7.
Thomas K, Engler AJ, Meyer GA (2015). Extracellular matrix regulation in the muscle satellite cell niche. Connect Tissue Res 56, 1–8.
Tierney MT, Gromova A, Sesillo FB, Sala D, Spenlé C, Orend G, Sacco A (2016). Autonomous extracellular matrix remodeling controls a progressive adaptation in muscle stem cell regenerative capacity during development. Cell Rep 14, 1940–1952.
Trensz F, Lucien F, Couture V, Söllrald T, Drouin G, Rouleau A-J, Grandbois M, Lacraz G, Grenier G (2015). Increased microenvironment stiffness in damaged myofibers promotes myogenic progenitor cell proliferation. Skelet Muscle 5.
Troy A, Cadwallader AB, Fedorov Y, Tyner K, Tanaka KK, Olwin BB (2012). Coordination of satellite cell activation and self-renewal by par-complex-dependent asymmetric activation of p38α/β MAPK. Cell Stem Cell 11, 541–553.
Urciuolo A, Quarta M, Morbidoni V, Gattazzo F, Molon S, Grumati P, Montemurro F, Tedesco FS, Blaauw B, Cossu G, *et al*. (2013). Collagen VI regulates satellite cell self-renewal and muscle regeneration. Nat Commun 4, 1964.
Webster MT, Manor U, Lippincott-Schwartz J, Fan C-M (2016). Intravital imaging reveals ghost fibers as architectural units guiding myogenic progenitors during regeneration. Cell Stem Cell 18, 243–252.
Wen JH, Vincent LG, Fuhrmann A, Choi YS, Hribar KC, Taylor-Weiner H, Chen S, Engler AJ (2014). Interplay of matrix stiffness and protein tethering in stem cell differentiation. Nat Mater 13, 979–987.
Yin H, Price F, Rudnicki MA (2013). Satellite cells and the muscle stem cell niche. Physiol Rev 93, 23–67.
Zammit PS, Golding JP, Nagata Y, Hudon V, Partridge TA, Beauchamp JR (2004). Muscle satellite cells adopt divergent fates: a mechanism for self-renewal? J Cell Biol 166, 347–357.